Turing pattern dynamics and adaptive discretization for a superdiffusive Lotka-Volterra system

Mostafa Bendahmane, Ricardo Ruiz-Baier, Canrong Tian

Journal of Mathematical Biology

Turing pattern dynamics and adaptive discretization for a superdiffusive Lotka-Volterra system

--Manuscript Draft--

Manuscript Number:	
Full Title:	Turing pattern dynamics and adaptive discretization for a superdiffusive Lotka-Volterra system
Article Type:	Original Research
Keywords:	Turing instability; Pattern formation; Amplitude equations; Superdiffusion; Finite volume approximation; Fully adaptive multiresolution
Corresponding Author:	Canrong Tian, Ph.D. Yangzhou, Jiangsu Province CHINA
Corresponding Author Secondary Information:	
Corresponding Author's Institution:	
Corresponding Author's Secondary Institution:	
First Author:	Mostafa Bendahmane, PhD
First Author Secondary Information:	
Order of Authors:	Mostafa Bendahmane, PhD
	Ricardo Ruiz-Baier, PhD
	Canrong Tian, Ph.D.
Order of Authors Secondary Information:	
Abstract:	We focus our attention on the effects of introducing the fractional-in-space operator into a Lotka-Volterra competitive model describing population superdiffusion. First, we address the weak solvability of the coupled problem employing the Faedo-Galerkin method and compactness arguments. In addition, we are interested in how cross superdiffusion influences the formation of spatial patterns: a linear stability analysis has been carried out, showing that cross superdiffusion triggers Turing instabilities, whereas classical self superdiffusion suppresses Turing instability. We have also performed a weakly nonlinear analysis yielding a system of amplitude equations, whose study shows the stability of Turing steady states. A second goal of this contribution is to propose a fully adaptive multiresolution finite volume (MRFV) method that employs shifted Grunwald gradient approximations, and which is tailored for a larger class of systems involving fractional diffusion operators, and aimed at efficient dynamic mesh adaptation and substantial savings in computational burden. A numerical simulation of the model was performed near the instability boundaries, confirming the behavior predicted by our analysis.
Suggested Reviewers:	Justin Tzou Northwestern University tzou.justin@gmail.com He is an expert in the field of fractional-in-space operator.
	Bernard J Matkowsky Northwestern University b-matkowsky@northwestern.edu He is an expert in the field of fractional-in-space operator.
	Raimund Burger Universidad de Concepcion

	rburger@ing-mat.udec.cl He is an expert in the field of fractional-in-space operator.
	Lai Zhang Umea University Lai.Zhang@math.umu.se He is an expert in Biomathematics.
	Zhigui Lin Yangzhou University zglin68@hotmail.com He is an expert in Biomathematics.

Journal of Mathematical Biology manuscript No.
(will be inserted by the editor)

Turing pattern dynamics and adaptive discretization for a superdiffusive Lotka-Volterra system

Mostafa Bendahmane · Ricardo Ruiz-Baier · Canrong Tian

July 23, 2014

Abstract We focus our attention on the effects of introducing the fractional-in-space operator into a Lotka-Volterra competitive model describing population superdiffusion. First, we address the weak solvability of the coupled problem employing the Faedo-Galerkin method and compactness arguments. In addition, we are interested in how cross superdiffusion influences the formation of spatial patterns: a linear stability analysis has been carried out, showing that cross superdiffusion triggers Turing instabilities, whereas classical *self* superdiffusion suppresses Turing instability. We have also performed a weakly nonlinear analysis yielding a system of amplitude equations, whose study shows the stability of Turing steady states. A second goal of this contribution is to propose a fully adaptive multiresolution finite volume (MRFV) method that employs shifted Grünwald gradient approximations, and which is tailored for a larger class of systems involving fractional diffusion operators, and aimed at efficient dynamic mesh adaptation and substantial savings in computational burden. A numerical simulation of the model was performed near the instability boundaries, confirming the behavior predicted by our analysis.

Keywords Turing instability · Pattern formation · Amplitude equations · Superdiffusion · Finite volume approximation · Fully adaptive multiresolution

Mathematics Subject Classification (2000) Primary 35B35 · Secondary 35B40 · 47D20

M. Bendahmane
Institut de Mathématiques de Bordeaux, Université Victor Segalen Bordeaux 2
33076 Bordeaux Cedex, France.
E-mail: mostafa.bendahmane@u-bordeaux2.fr

R. Ruiz-Baier
Institute of Earth Sciences, University of Lausanne
CH-1015, Lausanne, Switzerland.
E-mail: ricardo.ruizbaier@unil.ch

C. Tian
Department of Basic Sciences, Yancheng Institute of Technology
Yancheng 224003, China.
Corresponding author, E-mail: tiancanrong@163.com

1 Introduction

In population dynamics, a spatially homogeneous competitive system can be modelled with the so-called Lotka-Volterra system of differential equations written in the form

$$\frac{du}{dt} = u(a_1 - b_{11}u - b_{12}v),$$
$$\frac{dv}{dt} = v(a_2 - b_{21}u - b_{22}v).$$

In this model, u and v represent the population densities of two competitors, a_i are the birth (or generation) rates of the $i-$th population, the coefficients b_{ii} measure the intra-population competitive effect of the two competitors, $i = 1, 2$, and b_{12}, b_{21} stand for a factor representing the inter-population competitive effects of u on v, and of v on u, respectively.

As usual, we rescale the system variables:

$$\bar{u} = \frac{b_{11}}{a_1}u,\ \bar{v} = \frac{b_{22}}{a_1}v,\ \bar{t} = a_1 t,\ a = \frac{a_2}{a_1},\ b = \frac{b_{21}}{b_{11}},\ c = \frac{b_{12}}{b_{22}},$$

and after dropping the bars, we find that the interaction of u and v is governed by the following system of ordinary differential equations

$$\frac{du}{dt} = u(1 - u - cv), \qquad \frac{dv}{dt} = v(a - bu - v).$$

The population density in a spatially heterogeneous environment depends on space, where normal diffusive terms are usually introduced to the evolution system (see e.g. Okubo and Levin, 2002). As it is well-known, at molecular level, classical diffusion arises as the result of the standard Brownian motion, and it is typically characterized by the dependence of the mean square displacement of a randomly walking particle on time $\langle(\Delta x)^2\rangle \sim t$. Apart from classical (or normal) diffusion, molecules may undergo *anomalous* diffusion effects (Bouchard and Georges, 1990; Metzler and Klafter, 2000, 2004; Sokolov et al., 2002; Golovin et al., 2008; Gambino et al., 2013), which, in contrast to normal diffusion, need to be characterized by the more general dependence $\langle(\Delta x)^2\rangle = 2dK_\alpha t^\alpha$. Here d is the (embedding) spatial dimension, K_α is a generalized diffusion constant, and the exponent α is not necessarily an integer. For $\alpha = 1$, anomalous diffusion reduces to normal diffusion, with the classical diffusion coefficient set to K_1. For $\alpha < 1 (\alpha > 1)$, the diffusion process is slower (faster) than normal diffusion, in which case it is called sub-diffusive (resp., superdiffusive). An important limiting case of superdiffusion corresponds to Lévy flights (Metzler and Klafter, 2004), which is a phenomenon occurring in systems where there are long jumps of particles, i.e., with a jump size distribution having infinite moments. In the context of population dynamics, superdiffusion (rather than classical diffusion) has been employed as a more appropriate way to describe the motion of animals (Viswanathan and Afanasyevt, 1996; Schmitt and Seuront, 2001; Toner et al., 2005).

To take into account the movement of populations with Lévy flight type, we are led to the following fractional reaction diffusion system:

$$\begin{aligned} \partial_t u &= d_{11}\nabla^\gamma u + d_{12}\nabla^\gamma v + u(1 - u - cv), \\ \partial_t v &= d_{22}\nabla^\gamma v + v(a - bu - v). \end{aligned} \tag{1.1}$$

Here d_{11} and d_{22} are the self superdiffusive coefficients, and d_{12} is the cross superdiffusive coefficient. The so-called Weyl fractional operator ∇^γ $(1 < \gamma \leq 2)$ represents the superdiffusion, whose Fourier transform is $\widehat{\nabla^\gamma u}(\mathbf{k}) = -|\mathbf{k}|^\gamma \hat{u}(\mathbf{k})$. In one dimension, the Weyl operator is equivalent to the Riesz operator

$$\nabla^\gamma u = -\frac{1}{2\cos(\pi\gamma/2)}(D_+^\gamma u + D_-^\gamma u),$$

$$D_+^\gamma u = \frac{1}{\Gamma(2-\gamma)} \frac{d^2}{dx^2} \int_{-\infty}^{x} \frac{u(\xi,t)}{(x-\xi)^{\gamma-1}} d\xi,$$
$$D_-^\gamma u = \frac{1}{\Gamma(2-\gamma)} \frac{d^2}{dx^2} \int_{x}^{\infty} \frac{u(\xi,t)}{(\xi-x)^{\gamma-1}} d\xi,$$

where $\Gamma(\cdot)$ stands for the Gamma function. In higher dimensions, the Weyl operator can be represented by the fractional Laplacian operator $\nabla^\gamma = -(-\Delta)^{\gamma/2}$, and so system (1.1) can be written as

$$\begin{aligned} &\partial_t u + d_{11}(-\Delta)^{\gamma/2} u + d_{12}(-\Delta)^{\gamma/2} v = u(1-u-cv), \\ &\partial_t v + d_{22}(-\Delta)^{\gamma/2} v = v(a-bu-v). \end{aligned} \tag{1.2}$$

Pattern formation in reaction diffusion systems with anomalous diffusion has recently received considerable attention (Gafiychuk and Datsko, 2006; Henry et al., 2005; Henry and Wearne, 2002; Langlands et al., 2007; Weiss et al., 2003; Golovin et al., 2008; Gambino et al., 2013). For instance, it was shown that sub-diffusion suppresses the formation of Turing pattern (Weiss et al., 2003). It was also found in one dimensional systems that anomalous heat conduction can happen as a consequence of the anomalous diffusion (Li and Wang, 2003). Additionally, in systems with Lévy flights, the emergence of spiral waves and chemical turbulence from the nonlinear dynamics of oscillating reaction diffusion patterns was investigated in Nec et al. (2008). The authors in Golovin et al. (2008) explored the effects of superdiffusion on pattern formation and pattern selection in the substrate-depleted Brusselator model, and found that Turing instability can occur even when diffusion of the inhibitor is slower than that of the activator. However, results on the nonlinear dynamics and Turing pattern selection in reaction diffusion systems with cross superdiffusion remain limited.

The effect of pattern formation of the Lotka-Volterra competitive model with normal diffusion and cross diffusion has been extensively investigated (see Horstmann, 2007; Jüngel, 2010 for some reviews). In Lou and Ni (1996); Lou et al. (2001), the authors show that self diffusion tends to suppress pattern formation, whereas cross diffusion fosters the creation of patterns. In contrast, here we consider the effect of cross Lévy flights and superdiffusion on Turing patterns, and focus on the mode of pattern formation and the stability of the emerging patterns.

The remainder of this paper has been structured in the following way. Section 2 focuses on the weak solvability analysis of system (1.2), for which we use the well-known Faedo-Galerkin strategy and the Kruzhkov compactness result to establish the existence of weak solutions. In Section 3 we develop a linear stability analysis of the steady state of the system, which in turn provide the Turing parameter space that identifies regions where Turing bifurcations are expected. Section 4 is devoted to the derivation of a set of coupled amplitude equations, obtained by a weakly nonlinear analysis. Next, an analysis of these equations yields sufficient conditions to ensure so-called super-critical bifurcations, which we present in Section 5. There we also show how the stability of the Turing steady states is affected by these conditions. A fully adaptive finite volume – multiresolution method for the space-time discretization of (1.2) is proposed and discussed in Section 6. A simple numerical example is provided in Section 7, and we collect some closing remarks in Section 8.

2 Existence of weak solutions

Let Ω be a bounded open subset of $\mathbf{R}^d$ $(d = 2, 3)$ with a smooth (say C^2) boundary $\partial\Omega$. For $1 \le q < \infty$ and X is a Banach space, then $L^q(0,T;X)$ denotes the space of measurable function $u : (0,T) \to X$ for which $t \mapsto \|u(t)\|_X \in L^q(0,T)$. Moreover, $C([0,T];X)$ denotes the

space of continuous functions $u : [0,T] \to X$ for which $\|u\|_{C([0,T];X)} := \max_{t\in(0,T)} \|u(t)\|_X$ is finite.

The Fourier transform $\hat{u}$ of a tempered distribution $u(x)$ on Ω is defined by

$$\hat{u}(\mathbf{k}) = \frac{1}{(2\pi)^d} \int_\Omega \exp(-i\mathbf{k}\cdot x) u(x)\, dx.$$

Note that the fractional diffusion operator Λ^γ can be identified with the Fourier transform

$$\widehat{\Lambda^\gamma u}(\mathbf{k}) = |i\mathbf{k}|^\gamma\, \hat{u}(\mathbf{k}),$$

for $\gamma \in \mathbf{R}$. We denote by $H^\gamma(\Omega)$ the non-homogeneous fractional Sobolev space of functions u such that

$$\|u\|_{H^\gamma(\Omega)} = \Big(\sum_{\mathbf{k}\in\mathbf{Z}^d} (1+|\mathbf{k}|^2)^\gamma\, |\hat{u}(\mathbf{k})|^2 \Big)^{\frac{1}{2}} < \infty.$$

The homogeneous fractional Sobolev space of functions u is denoted by $\tilde{H}^\gamma(\Omega)$ given by

$$\|u\|_{\tilde{H}^\gamma(\Omega)} = \Big(\sum_{\mathbf{k}\in\mathbf{Z}^d} |\mathbf{k}|^{2\gamma}\, |\hat{u}(\mathbf{k})|^2 \Big)^{\frac{1}{2}} < \infty.$$

Next, we define $-\Delta : H_0^1(\Omega) \to L^2(\Omega)$ with domain:

$$\mathrm{Dom}(-\Delta) = \{u \in H_0^1(\Omega) \text{ such that } \Delta u \in L^2(\Omega)\}.$$

Note that the operator $A = -\Delta$ is positive, unbounded, closed and its inverse is compact. This implies

$$Aw_\ell = \lambda_\ell\, w_\ell,$$

for $w_\ell \in \mathrm{Dom}(-\Delta)$, where $\{w_\ell\}_{\ell=1}^\infty$. are the eigenfunctions (orthogonal basis of $H_0^1(\Omega)$) with the corresponding eigenvalues $\{\lambda_\ell\}_{\ell=1}^\infty$.

With this spectral decomposition the fractional powers of the Dirichlet fractional Laplacian Λ^γ ($\Lambda = (-\Delta)^{1/2}$, $1 < \gamma \le 2$) can be defined for $u \in C_0^\infty(\Omega)$ by

$$(-\Delta)^{\gamma/2} u = \Lambda^\gamma u = \sum_{\ell=1}^\infty u_\ell\, \lambda_\ell^{\gamma/2}\, w_\ell$$

where the coefficients u_ℓ are defined by $u_\ell = \int_\Omega u w_\ell$.

Now we define what we mean by weak solutions of the system (1.2) completed with Dirichlet boundary conditions and initial conditions on u, v:

Definition 21 *A weak solution of (1.2) is a set of nonnegative functions (u,v) such that,*

a) $(u,v) \in L^\infty(0,T; L^2(\Omega,\mathbf{R}^d)) \cap L^2(0,T;\tilde{H}^{\gamma/2}(\Omega,\mathbf{R}^d))$,
b) $F(u,v), G(u,v) \in L^1((0,T)\times\Omega)$, $u(0,\cdot) = u_0(\cdot)$ *and* $v(0,\cdot) = v_0(\cdot)$ *a.e. in* Ω,
c) $Q_T = \Omega \times [0,T]$ *and they satisfy*

$$-\iint_{Q_T} u\partial_t\varphi_1\, dx\, dt + d_{11} \iint_\Omega \Lambda^{\gamma/2}u \cdot \Lambda^{\gamma/2}\varphi_1\, dx\, dt + d_{12} \iint_\Omega \Lambda^{\gamma/2}v \cdot \Lambda^{\gamma/2}\varphi_1\, dx\, dt$$
$$= -\int_\Omega u_0(x)\varphi_1(0,x)\, dx + \iint_{Q_T} F(u,v)\varphi_1\, dx\, dt,$$
$$-\iint_{Q_T} v\partial_t\varphi_2\, dx\, dt + d_{22} \iint_\Omega \Lambda^{\gamma/2}v \cdot \Lambda^{\gamma/2}\varphi_2\, dx\, dt$$
$$= -\int_\Omega u_0(x)\varphi_1(0,x)\, dx + \iint_{Q_T} G(u,v)\varphi_2\, dx\, dt,$$

for all $\varphi_1, \varphi_2 \in \mathcal{D}([0,T)\times\Omega)$, *where* $F(u,v) = u(1-u-c\,v)$ *and* $G(u,v) = v(a - b\,u - v)$.

Theorem 1 *If $(u_0, v_0) \in L^2(\Omega, \mathbf{R}^d)$, then problem (1.2) possesses a weak solution in the sense of Definition 21.*

The proof of Theorem 1 (the existence of weak solution) is based on Faedo-Galerkin method. Although the existence proof for (1.2) will be the subject of a separate contribution, we outline in what follows the main steps. We look for finite dimensional approximate solution to the problem (1.2) (we complete the system (1.2) with Dirichlet boundary conditions and initial conditions on u, v): as sequences $(u_n)_{n>1}$, $(v_n)_{n>1}$ defined for $t \geq 0$ and $x \in \overline{\Omega}$ by

$$u_n(t,x) = \sum_{l=1}^{n} b_{n,l}(t) e_l(x), \qquad v_n(t,x) = \sum_{l=1}^{n} c_{n,l}(t) e_l(x). \tag{2.1}$$

The next step is to determine the coefficients $(b_{n,l}(t))_{l=1}^n$, $(c_{n,l}(t))_{l=1}^n$ such that for $k = 1, \ldots, n$ it holds

$$\begin{aligned} (\partial_t u_n, e_k)_{L^2(\Omega)} + d_{11} \int_\Omega \Lambda^{\gamma/2} u_n \cdot \Lambda^{\gamma/2} e_k \, dx & \\ + d_{12} \int_\Omega \Lambda^{\gamma/2} v_n \cdot \Lambda^{\gamma/2} e_k \, dx &= \int_\Omega F(u_n^+, v_n^+) e_k \, dx, \\ (\partial_t v_n, e_k)_{L^2(\Omega)} + d_{22} \int_\Omega \Lambda^{\gamma/2} v_n \cdot \Lambda^{\gamma/2} e_k \, dx &= \int_\Omega G(u_n^+, v_n^+) e_k \, dx, \end{aligned} \tag{2.2}$$

and regarding to the initial conditions,

$$\begin{aligned} u_n(0,x) = u_{0,n}(x) := \sum_{l=1}^{n} b_{n,l}(0) e_l(x), \qquad & b_{n,l}(0) := (u_0, e_l)_{L^2(\Omega)}, \\ v_n(0,x) = v_{0,n}(x) := \sum_{l=1}^{n} c_{n,l}(0) e_l(x), \qquad & c_{n,l}(0) := (v_0, e_l)_{L^2(\Omega)}. \end{aligned}$$

Herein

$$F(u_n^+, v_n^+) = u_n^+(1 - u_n^+ - c\, v_n^+) \text{ and } G(u_n^+, v_n^+) = v_n^+(a - b\, u_n^+ - v_n^+),$$

where $w^+ = \max(0, -w)$ for $w = u, v$.

Observe that, since $u_0, v_0 \in L^2(\Omega)$, it is clearly seen that as $n \to \infty$, $u_{0,n} \to u_0$ and $v_{0,n} \to v_0$ in $L^2(\Omega)$, respectively. Using the normality of the respective basis, we can write (2.2) as a system of ordinary differential equations:

$$\begin{aligned} b'_{n,k}(t) + d_{11} \int_\Omega \Lambda^{\gamma/2} u_n \cdot \Lambda^{\gamma/2} e_k \, dx & \\ + d_{12} \int_\Omega \Lambda^{\gamma/2} v_n \cdot \Lambda^{\gamma/2} e_k \, dx &= \int_\Omega F(u_n^+, v_n^+) e_k \, dx, \\ c'_{n,k}(t) + d_{22} \int_\Omega \Lambda^{\gamma/2} v_n \cdot \Lambda^{\gamma/2} e_k \, dx &= \int_\Omega G(u_n^+, v_n^+) e_k \, dx. \end{aligned}$$

Let $\mathcal{F}$ and $\mathcal{G}$ be functions defined as follow:

$$\begin{aligned} \mathcal{F}(t, (b_{n,l}(t))_{l=1}^n, (c_{n,l}(t))_{l=1}^n) := \int_\Omega F(u_n^+, v_n^+) e_k \, dx - d_{11} \int_\Omega \Lambda^{\gamma/2} u_n \cdot \Lambda^{\gamma/2} e_k \, dx & \\ - d_{12} \int_\Omega \Lambda^{\gamma/2} v_n \cdot \Lambda^{\gamma/2} e_k \, dx, & \\ \mathcal{G}(t, (b_{n,l}(t))_{l=1}^n, (c_{n,l}(t))_{l=1}^n) := \int_\Omega G(u_n^+, v_n^+) e_k \, dx - d_{22} \int_\Omega \Lambda^{\gamma/2} v_n \cdot \Lambda^{\gamma/2} e_k \, dx. & \end{aligned}$$

Proceeding in an analogous way to the developments in Andreianov et al. (2011); Bendahmane (2010); Bendahmane and Karlsen (2006), we can prove that $\mathcal{F}$ and $\mathcal{G}$ are Carathéodory functions, and we can show an existence interval $[0,t')$ for the Faedo-Galerkin solutions u_n and v_n defined by (2.1).
On the other hand, to prove global existence of the solutions we derive n-independent a priori estimates bounding u_n, v_n in various Banach spaces. Given some continuous coefficients $d_{1,n,l}(t)$ and $d_{2,n,l}(t)$, we form the functions $\varphi_{1,n}(t,x) := \sum_{l=1}^{n} d_{1,n,l}(t)e_l(x)$ and $\varphi_{2,n}(t,x) := \sum_{l=1}^{n} d_{2,n,l}(t)e_l(x)$. Now our Faedo-Galerkin solutions satisfy the following weak formulations:

$$\int_\Omega \partial_s u_n \varphi_{1,n}\,dx + d_{11}\int_\Omega \Lambda^{\gamma/2}u_n\cdot\Lambda^{\gamma/2}\varphi_{1,n}\,dx + d_{12}\int_\Omega \Lambda^{\gamma/2}v_n\cdot\Lambda^{\gamma/2}\varphi_{1,n}\,dx = \int_\Omega F(u_n^+,v_n^+)\varphi_{1,n}\,dx, \tag{2.3}$$

$$\int_\Omega \partial_s v_n \varphi_{2,n}\,dx + d_{22}\int_\Omega \Lambda^{\gamma/2}v_n\cdot\Lambda^{\gamma/2}\varphi_{2,n}\,dx = \int_\Omega G(u_n^+,v_n^+)\varphi_{2,n}\,dx. \tag{2.4}$$

Now, we substitute $\varphi_{1,n} = u_n$ and $\varphi_{1,n} = u_n$ in (2.3) and (2.4), respectively. Then integrating over $(0,t)$ and using Young and Gronwall inequalities, we get for $t \in [0,t')$

$$\|v_n\|_{L^\infty(0,t;L^2(\Omega))} \le C,$$
$$\int_0^t\int_\Omega \left|\Lambda^{\gamma/2}u_n\right|^2\,dx\,ds + \int_0^t\int_\Omega \left|\Lambda^{\gamma/2}v_n\right|^2\,dx\,ds \le C,$$

for some constant $C>0$ not depending on n.

The next step is to show that the local solution constructed above can be actually extended to the whole time interval $[0,T)$ (independent of n). We stress that this can be done as in Bendahmane and Karlsen (2006), so we omit the details.

Now, if we choose $\varphi_{1,n} = -u_n^-$, $\varphi_{2,n} = -v_n^-$ in (2.3) and (2.4), respectively, then after integration over $(0,t)$ with $0 < t \le T$, we readily obtain the non-negativity of the solution (u_n, v_n).

With the help of a compactness tool inspired by Kruzhkov lemma (Kruzhkov, 1969), we justify that the solutions (u_n, v_n) is relatively compact in $L^1(Q_T)$. From this we can extract subsequences, which we do not relabel and we can assume that there exist limit functions u, v such that as $n \to \infty$

$$\begin{cases} u_n \to u, v_n \to v \text{ strongly in } L^1(Q_T) \text{ and a.e. in } Q_T,\\ u_n \rightharpoonup u, v_n \rightharpoonup v \text{ weakly in } L^2(0,T;\tilde{H}^\gamma(\Omega)),\\ F(u_n,v_n)\to F(u,v), G(u_n,v_n)\to G(u,v) \text{ in } L^1(Q_T) \text{ a.e. in } Q_T. \end{cases} \tag{2.5}$$

Keeping in mind (2.5) and using the following weak formulation:

$$\begin{aligned} -\int\int_{Q_T} u_n\partial_t\varphi_1\,dx\,dt + d_{11}\iint_\Omega \Lambda^{\gamma/2}u_n\cdot\Lambda^{\gamma/2}\varphi_{1,n}\,dx\,dt \\ + d_{12}\iint_\Omega \Lambda^{\gamma/2}v_n\cdot\Lambda^{\gamma/2}\varphi_{1,n}\,dx\,dt \\ = -\int_\Omega u_0(x)\varphi_1(0,x)\,dx + \iint_{Q_T} F(u_n,v_n)\varphi_1\,dx\,dt, \\ -\int\int_{Q_T} v_n\partial_t\varphi_2\,dx\,dt + d_{22}\iint_\Omega \Lambda^{\gamma/2}v_n\cdot\Lambda^{\gamma/2}\varphi_{2,n}\,dx\,dt \\ = -\int_\Omega u_0(x)\varphi_1(0,x)\,dx + \iint_{Q_T} G(u_n,v_n)\varphi_2\,dx\,dt, \end{aligned}$$

for all $\varphi_1, \varphi_2 \in \mathcal{D}([0,T)\times\Omega)$, we can let $n\to\infty$ and obtain a weak solution.

3 Linear stability analysis

In this section, we provide essential conditions to drive the Turing bifurcation by analyzing the linear stability of the uniform equilibrium state of (1.1). Notice that system (1.1) has a unique positive equilibrium $(u^*, v^*) = (\frac{1-ac}{1-bc}, \frac{a-b}{1-bc})$ if and only if

$$b < a < \frac{1}{c}. \tag{3.1}$$

Moreover, one can readily verify that (3.1) ensures that the positive equilibrium (u^*, v^*) is stable under any spatially homogeneous perturbation.

In order to carry out the linear stability analysis of (1.1), we set $\bar{u} = u - u^*$, $\bar{v} = v - v^*$, and substitute them in the system (1.1). By dropping the bars, we can write the linearized form of the system (1.1) at the positive equilibrium as follows:

$$\begin{aligned} \partial_t u &= d_{11}\nabla^\gamma u + d_{12}\nabla^\gamma v - u^* u - cu^* v - u^2 - cuv, \\ \partial_t v &= d_{22}\nabla^\gamma v - bv^* u - v^* v - buv - v^2. \end{aligned} \tag{3.2}$$

Let us further assume that the perturbation of (1.1) is periodic with respect to time. Hence the conditions of the classical Fourier theorem are met, and we seek the general solution

$$\begin{pmatrix} u \\ v \end{pmatrix} = \begin{pmatrix} c_1 \\ c_2 \end{pmatrix} \exp(\sigma t + i\mathbf{k}\cdot x) \tag{3.3}$$

to the linearization of the problem (3.2) as a superposition of normal modes. Here σ is the growth rate of the perturbation in time t, i denotes the imaginary unit, with $i^2 = -1$, and $\mathbf{k}$ is its wave vector. Suggested by the definition of the Weyl fractional operator ∇^γ, we focus on the time integration in Fourier space. Substituting (3.3) into the linearization of Eqs. (3.2), we obtain the following matrix equation

$$\begin{pmatrix} \sigma + u^* + d_{11}k^\gamma & cu^* + d_{12}k^\gamma \\ bv^* & \sigma + v^* + d_{22}k^\gamma \end{pmatrix} \begin{pmatrix} c_1 \\ c_2 \end{pmatrix} = \begin{pmatrix} 0 \\ 0 \end{pmatrix},$$

where the Euclidean norm $k = |\mathbf{k}|$ is the wavenumber of the perturbation. Therefore, we are left to the dispersion relation

$$\sigma^2 + g(k)\sigma + h(k) = 0,$$

where

$$\begin{aligned} g(k) &:= u^* + v^* + (d_{11} + d_{22})k^\gamma, \\ h(k) &:= d_{11}d_{22}k^{2\gamma} + (d_{11}v^* + d_{22}u^* - d_{12}bv^*)k^\gamma + (1 - bc)u^*v^*. \end{aligned}$$

We stress that the corresponding equilibrium can lose its stability via Turing bifurcation if and only if $h(k) \le 0$. Moreover, note that in the absence of cross superdiffusion one has $h(k) > 0$, which implies that in this particular case, only the cross superdiffusion effect can induce Turing bifurcation. Notice that $h(k)$ has a single minimum (k_c, d_{12}^c), which is attained whenever

$$\begin{aligned} d_{12}^c &= \frac{d_{11}v^* + d_{22}u^* + 2\sqrt{(1-bc)d_{11}d_{22}u^*v^*}}{bv^*}, \\ k_c &= \left(\frac{\sqrt{(1-bc)u^*v^*}}{\sqrt{d_{11}d_{22}}}\right)^{\frac{1}{\gamma}}. \end{aligned} \tag{3.4}$$

Summarizing, we have obtained a Turing instability threshold d_{12}^c, and we have identified the critical value of the wave number k_c. Relation (3.4) represents the bifurcations occurrying

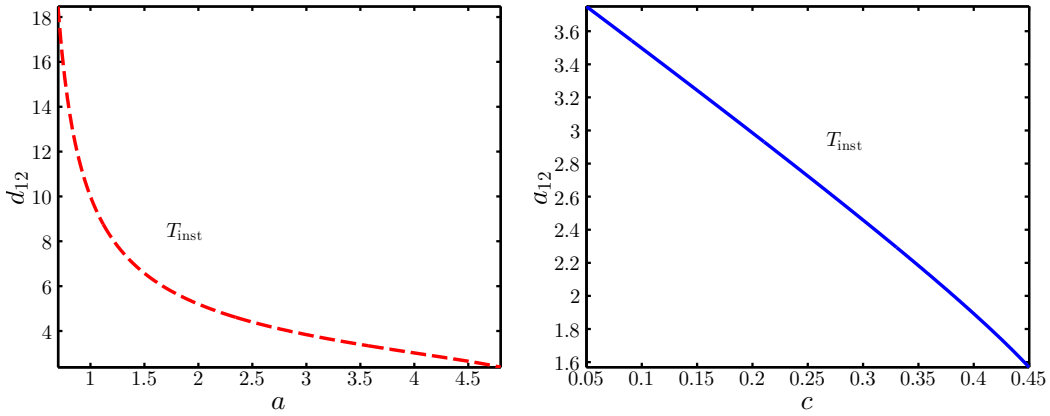

Fig. 1 Turing instability boundaries in the (a, d_{12}) and (c, d_{12}) planes. The instability region T_{inst} lies above the curves.

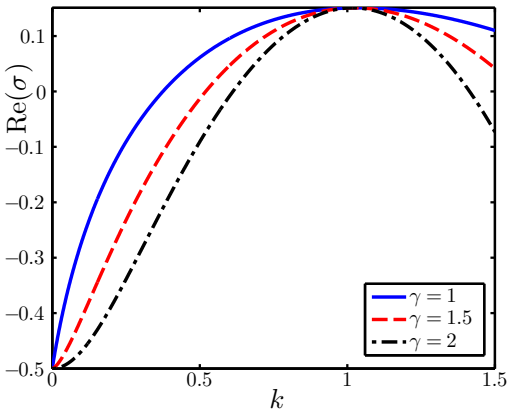

Fig. 2 Dispersion relation of the system (1.1) for three different $\gamma = 1,\ 1.5,\ 2$. The other parameters are $a = 2$, $b = 1$, $c = 0.2$, $d_{11} = 1$, $d_{22} = 1$, and $d_{12} = 3.5$.

in the parameter region spanned by the parameters a, c and d_{12}. These regimes are also depicted in Figure 1. All Turing patterns are driven by parameters chosen in this region. In addition, Figure 2 displays the real part of the eigenvalue corresponding to three different sets of parameters, as a function of the wavenumber, and we notice that the active wavenumber does not change with the order of the fractional diffusion γ.

4 Weakly nonlinear analysis

In order to study the dynamics of Turing patterns, we perform here a weakly nonlinear analysis of system (3.2) near the Turing instability threshold. In particular, we aim at analyzing the pattern selection mechanisms associated to hexagons and stripes. Let us consider system (3.2) defined in the whole two-dimensional space $\mathbf{R}^2$. Weakly nonlinear analyses are typically based on the fact that Turing bifurcations are able to destabilize the homogeneous equilibrium, but only in case of perturbations with wave numbers close to the critical value k_c. In regimes near to the Turing onset $d_{12} = d_{12}^c$, the solutions can be described by a system of three active resonant pairs of modes $(\mathbf{k_j}, \ -\mathbf{k_j})$, for $j = 1, 2, 3$. Each pair of modes form angles of $2\pi/3$

and $|\mathbf{k_j}| = k_c$. This fact implies that solutions of system (3.2) can be expanded as

$$\begin{pmatrix} u \\ v \end{pmatrix} = \sum_{j=1}^{3} [\mathbf{A_j} \exp(i\mathbf{k_j} \cdot x + \bar{\mathbf{A}}_\mathbf{j} \exp(-i\mathbf{k_j} \cdot x)], \tag{4.1}$$

where $\mathbf{A_j}$ and its conjugate $\bar{\mathbf{A}}_\mathbf{j}$ stand, respectively, for the amplitudes associated with the modes $\mathbf{k_j}$ and $-\mathbf{k_j}$, and $\mathbf{A_j} \equiv (A_j^u, A_j^v)^T$.

We introduce a scaled *slow* time variable $T = \varepsilon^2 t$, and expand both fields u and v, as well as the bifurcation parameter d_{12}, in the form

$$\begin{aligned} \begin{pmatrix} u \\ v \end{pmatrix} &= \varepsilon \begin{pmatrix} u_1 \\ v_1 \end{pmatrix} + \varepsilon^2 \begin{pmatrix} u_2 \\ v_2 \end{pmatrix} + \varepsilon^3 \begin{pmatrix} u_3 \\ v_3 \end{pmatrix} + \cdots, \\ d_{12} - d_{12}^c &= \mu_2 \varepsilon^2 + O(\varepsilon^3). \end{aligned} \tag{4.2}$$

Since the amplitude $\mathbf{A}$ is a variable that undergoes slow changes, it follows that

$$\partial_t \mathbf{A} = \varepsilon^2 \frac{\partial \mathbf{A}}{\partial T} + O(\varepsilon^3).$$

Substituting Equations (4.2) into the system (3.2), we have

$$\begin{aligned} \varepsilon^3 \frac{\partial}{\partial T} \begin{pmatrix} u_1 \\ v_1 \end{pmatrix} = \varepsilon \mathbf{L_c} \begin{pmatrix} u_1 \\ v_1 \end{pmatrix} + \varepsilon^2 \mathbf{L_c} \begin{pmatrix} u_2 \\ v_2 \end{pmatrix} + \varepsilon^3 \mathbf{L_c} \begin{pmatrix} u_3 \\ v_3 \end{pmatrix} - \varepsilon^3 \mu_2 k_c^\gamma \mathbf{M} \begin{pmatrix} u_1 \\ v_1 \end{pmatrix} \\ -\varepsilon^2 \begin{pmatrix} u_1^2 + c u_1 v_1 \\ b u_1 v_1 + v_1^2 \end{pmatrix} - \varepsilon^3 \begin{pmatrix} 2u_1 u_2 + c u_1 v_2 + c u_2 v_1 \\ b u_1 v_2 + b u_2 v_1 + 2 v_1 v_2 \end{pmatrix}, \end{aligned}$$

where the involved matrices are defined as

$$\mathbf{L_c} = \begin{pmatrix} -u^* + d_{11}\nabla^\gamma & -cu^* + d_{12}^c \nabla^\gamma \\ -bv^* & -v^* + d_{22}\nabla^\gamma \end{pmatrix}, \ \mathbf{M} = \begin{pmatrix} 0 & 1 \\ 0 & 0 \end{pmatrix}.$$

After collecting like powers of ε, we obtain the following systems, arranged according to the orders ε^j, $j = 1, 2, 3$

$$\begin{aligned} &O(\varepsilon) : \mathbf{L_c} \begin{pmatrix} u_1 \\ v_1 \end{pmatrix} = 0, \\ &O(\varepsilon^2) : \mathbf{L_c} \begin{pmatrix} u_2 \\ v_2 \end{pmatrix} = \begin{pmatrix} u_1^2 + c u_1 v_1 \\ b u_1 v_1 + v_1^2 \end{pmatrix}, \\ &O(\varepsilon^3) : \mathbf{L_c} \begin{pmatrix} u_3 \\ v_3 \end{pmatrix} = \frac{\partial}{\partial T} \begin{pmatrix} u_1 \\ v_1 \end{pmatrix} + \mu_2 k_c^\gamma \mathbf{M} \begin{pmatrix} u_1 \\ v_1 \end{pmatrix} \\ &\quad + \begin{pmatrix} 2u_1 u_2 + c u_1 v_2 + c u_2 v_1 \\ b u_1 v_2 + b u_2 v_1 + 2 v_1 v_2 \end{pmatrix}. \end{aligned} \tag{4.3}$$

Our next goal is to describe the appearance of both hexagonal and stripped spatial distributions as well as their spatio-temporal interactions. Since $\mathbf{L_c}$ is the linear operator of the system at the Turing instability threshold, it holds that $(u_1, v_1)^T$ is the linear combination of the eigenvectors corresponding to the null eigenvalue. Therefore, at $O(\varepsilon)$ the solution of the system exhibits the following structure

$$\begin{pmatrix} u_1 \\ v_1 \end{pmatrix} = \begin{pmatrix} -K_1 \\ 1 \end{pmatrix} \sum_{j=1}^{3} W_j \exp(i\mathbf{k_j} \cdot x) + c.c.,$$

where

$$K_1 = \frac{v^* + \sqrt{(1 - bc) u^* v^* d_{22}/d_{11}}}{bv^*},$$

and W_j is the amplitude of the mode $\exp(i\mathbf{k_j}\cdot x)$ when the system is under the first-order perturbation. Its form is determined by the perturbation term of highest order. The addition of the complex conjugate *c.c.* allows $(u_1, v_1)^T$ to be real.

Next, we turn to the term of $O(\varepsilon^2)$. Since the right-hand side does not exhibit resonance-related terms, the solution is given simply by

$$\begin{pmatrix} u_2 \\ v_2 \end{pmatrix} = \begin{pmatrix} U_0 \\ V_0 \end{pmatrix} + \begin{pmatrix} U_j \\ V_j \end{pmatrix} \sum_{j=1}^{3} \exp(i\mathbf{k_j}\cdot x) + c.c.$$

On the other hand, substitution of the above equation into the second equation of problem (4.3) yields

$$\begin{aligned} &\mathbf{L_c}\begin{pmatrix} U_0 \\ V_0 \end{pmatrix} + \sum_{j=1}^{3} \exp(i\mathbf{k_j}\cdot x)\mathbf{L_c}\begin{pmatrix} U_j \\ V_j \end{pmatrix} + \sum_{j=1}^{3} \exp(-i\mathbf{k_j}\cdot x)\mathbf{L_c}\begin{pmatrix} \bar{U}_j \\ \bar{V}_j \end{pmatrix} \\ &= (|W_1|^2 + |W_2|^2 + |W_3|^2)\begin{pmatrix} 2K_1^2 - 2cK_1 \\ 2 - 2bK_1 \end{pmatrix} + \sum_{j=1}^{3} O(\exp(2i\mathbf{k_j}\cdot x)) \\ &+ O(\exp(i(\mathbf{k_1}-\mathbf{k_2})\cdot x)) + O(\exp(i(\mathbf{k_2}-\mathbf{k_3})\cdot x)) + O(\exp(i(\mathbf{k_3}-\mathbf{k_1})\cdot x)) + c.c., \end{aligned}$$

and after collecting terms of orders $O(1)$ and $O(\exp(i\mathbf{k_j}x))$, we obtain

$$\begin{aligned} \begin{pmatrix} U_0 \\ V_0 \end{pmatrix} &= (|W_1|^2 + |W_2|^2 + |W_3|^2)\begin{pmatrix} -K_2 \\ 1 \end{pmatrix}, \\ K_2 &= \frac{v^{*2} + (v^*-2)\sqrt{(1-bc)u^*v^*d_{22}/d_{11}}}{bv^{*2}},\ U_j = -K_1V_j. \end{aligned}$$

We now turn to the term of $O(\varepsilon^3)$. According to the Fredholm solvability condition, the vector function of the right-hand side must be orthogonal with the zero eigenvalues of the operator $\mathbf{L_c^+}$ in order to ensure the existence of a nontrivial solution to this equation, where $\mathbf{L_c^+}$ is the adjoint operator of $\mathbf{L_c}$. The nontrivial kernel of the operator $\mathbf{L_c^+}$ is

$$\begin{pmatrix} 1 \\ -K_3 \end{pmatrix}\exp(-i\mathbf{k_j}x),\ K_3 = \frac{u^* + \sqrt{(1-bc)u^*v^*d_{11}/d_{22}}}{bv^*}.$$

Substituting the solution $(u_1, v_1)^T$ and $(u_2, v_2)^T$ into the problem containin the $O(\varepsilon^3)$ term, and applying Fredholm solvability condition, we can assert that

$$\begin{aligned} -(K_1+K_3)\frac{\partial W_1}{\partial T} &= -\mu_2 k_c^\gamma W_1 - [2K_1(K_1-c) - 2K_3(1-bK_1)](\bar{W}_2\bar{V}_3 + \bar{V}_2\bar{W}_3) \\ &\quad - [2K_1K_2 - cK_1 - cK_2 - K_3(2-bK_1-bK_2)]W_1(|W_1|^2 + |W_2|^2 + |W_3|^2). \end{aligned} \tag{4.4}$$

In view of (4.1) and (4.2), the amplitude A_j^v can be expanded as

$$\begin{aligned} A_j^v &= \varepsilon W_j + \varepsilon^2 V_j + O(\varepsilon^3), \quad j = 1,2,3, \\ \partial_t A_j^v &= \varepsilon^3 \frac{\partial W_j}{\partial T} + O(\varepsilon^4). \end{aligned}$$

Multiplying (4.4) by $-\varepsilon^3$, we get

$$\begin{aligned} (K_1+K_3)\partial_t A_1^v &= \varepsilon^2\mu_2 k_c^\gamma A_1^v + [2K_1(K_1-c) - 2K_3(1-bK_1)]\bar{A}_2^v\bar{A}_3^v \\ &\quad - [cK_1 + cK_2 + K_3(2-bK_1-bK_2) \\ &\quad - 2K_1K_2]A_1^v(|A_1^v|^2 + |A_2^v|^2 + |A_3^v|^2). \end{aligned} \tag{4.5}$$

In addition, multiplying (4.5) by $\frac{1}{k_c^\gamma d_{12}^c}$, we have the following amplitude equation

$$\tau_0 \partial_t A_1^v = \mu A_1^v + h \bar{A}_2^v \bar{A}_3^v - [g_1 |A_1^v|^2 + g_2(|A_2^v|^2 + |A_3^v|^2)] A_1^v, \tag{4.6}$$

where $\mu = \frac{d_{12} - d_{12}^c}{d_{12}^c}$ is a normalized distance to the Turing instability threshold, and $\tau_0 = \frac{K_1 + K_3}{k_c^\gamma d_{12}^c}$ is a typical relaxation time. Moreover,

$$\begin{aligned} h &= \frac{2K_1(K_1 - c) - 2K_3(1 - bK_1)}{k_c^\gamma d_{12}^c}, \\ g_1 = g_2 &= \frac{cK_1 + cK_2 + K_3(2 - bK_1 - bK_2) - 2K_1K_2}{k_c^\gamma d_{12}^c}. \end{aligned} \tag{4.7}$$

The remaining equations for A_2^v and A_3^v can be obtained analogously, through transformation of the subscript of A^v.

5 Stability of inhomogeneous patterns

In order to study the pattern selection, we need to analyze further the amplitude equation (4.6), where each amplitude can be decomposed into a mode $\rho_j = |A_j^v|$ and a corresponding phase angle φ_j. We proceed to rewrite (4.6) and the other two associated amplitude equations for $A_j^v = \rho_j \exp(i\varphi_j)$ in the following form:

$$\begin{aligned} \tau_0 \partial_t \Phi &= -h \frac{\rho_1^2\rho_2^2 + \rho_1^2\rho_3^2 + \rho_2^2\rho_3^2}{\rho_1\rho_2\rho_3} \sin\Phi, \\ \tau_0 \partial_t \rho_1 &= \mu\rho_1 + h\rho_2\rho_3 \cos\Phi - g_1\rho_3 - g_2(\rho_2^2 + \rho_3^2)\rho_1, \\ \tau_0 \partial_t \rho_2 &= \mu\rho_2 + h\rho_1\rho_3 \cos\Phi - g_1\rho_2 - g_2(\rho_1^2 + \rho_3^2)\rho_2, \\ \tau_0 \partial_t \rho_3 &= \mu\rho_3 + h\rho_1\rho_2 \cos\Phi - g_1\rho_3 - g_2(\rho_1^2 + \rho_2^2)\rho_3, \end{aligned} \tag{5.1}$$

where $\Phi = \phi_1 + \phi_2 + \phi_3$. The above equations imply that when the system is at steady state, the sum of the amplitude-phases only attains two values $\Phi = 0$ and $\Phi = \pi$. The fact that $\rho_j > 0$ for $j = 1, 2, 3$, implies that in the case $\Phi = 0$, the solutions of Eq. (5.1) are stable when $h > 0$; whereas for $\Phi = \pi$, the solutions of Eq. (5.1) are stable when $h < 0$. If we consider only the stable solutions of Eq. (5.1), then the mode equations can be recast in the form:

$$\tau_0 \frac{d\rho_1}{dt} = \mu\rho_1 + |h|\rho_2\rho_3 - g_1\rho_1^3 - g_2(\rho_2^2 + \rho_3^2)\rho_1, \tag{5.2}$$

$$\tau_0 \frac{d\rho_2}{dt} = \mu\rho_2 + |h|\rho_1\rho_3 - g_1\rho_2^3 - g_2(\rho_1^2 + \rho_3^2)\rho_2, \tag{5.3}$$

$$\tau_0 \frac{d\rho_3}{dt} = \mu\rho_3 + |h|\rho_1\rho_2 - g_1\rho_3^3 - g_2(\rho_1^2 + \rho_2^2)\rho_3. \tag{5.4}$$

Notice that the quadratic terms in (5.2)-(5.4) are positive, which is the main cause of instability in the linear term. In order to ensure that mode equations possess a steady state solution, the coefficients of cubic terms must be positive, which translates in imposing the following conditions

$$cK_1 + cK_2 + K_3(2 - bK_1 - bK_2) > 2K_1K_2,$$

that in turn yield supercritical Turing bifurcations in system (1.1). Otherwise, the weakly nonlinear analysis requires to be extended by expanding the Taylor series in (4.3) up to the fifth order so that the instability is covered (that is, (5.1) holds). The latter case corresponds to the so-called subcritical Turing bifurcation, which we do not consider in the present paper. Figure 3 displays the Turing bifurcation diagram in the (b, a) plane.

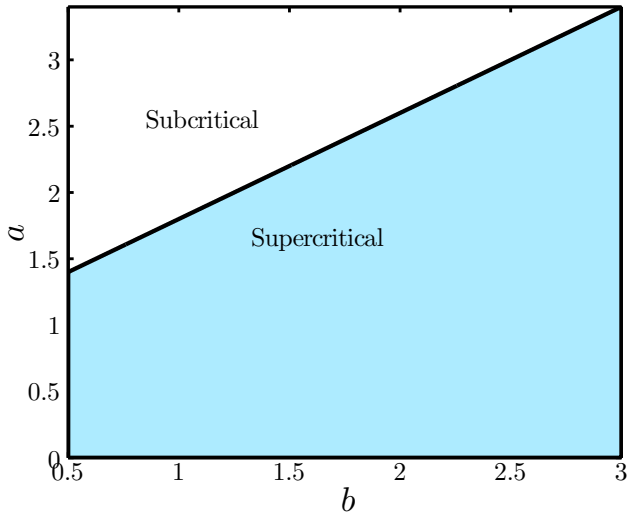

Fig. 3 Turing bifurcation diagram. The shaded region represents the supercritical states, whereas the white region is subcritical zone. The remaining parameters are $c = 0.2$, $d_{11} = 1$, and $d_{22} = 1$.

In order to assess the stability of the mode equations, we add a perturbation $(\delta\rho_1, \delta\rho_2, \delta\rho_3)$ to the steady state (ρ_1, ρ_2, ρ_3) and substitute it into Eqs. (5.2)-(5.4). Retaining the linear terms, we end up with the linear perturbation equations:

$$\tau_0 \frac{d}{dt}\begin{pmatrix}\delta\rho_1\\ \delta\rho_2\\ \delta\rho_3\end{pmatrix} = \mathbf{J}\begin{pmatrix}\delta\rho_1\\ \delta\rho_2\\ \delta\rho_3\end{pmatrix},$$
$$\text{where } \mathbf{J} = \begin{pmatrix} \mu - 3g_1\rho_1^2 - g_2(\rho_2^2+\rho_3^2) & |h|\rho_3 - 2g_2\rho_1\rho_2 & |h|\rho_2 - 2g_2\rho_1\rho_3 \\ |h|\rho_3 - 2g_2\rho_1\rho_2 & \mu - 3g_1\rho_2^2 - g_2(\rho_1^2+\rho_3^2) & |h|\rho_1 - 2g_2\rho_2\rho_3 \\ |h|\rho_2 - 2g_2\rho_1\rho_3 & |h|\rho_1 - 2g_2\rho_2\rho_3 & \mu - 3g_1\rho_3^2 - g_2(\rho_1^2+\rho_2^2) \end{pmatrix}. \tag{5.5}$$

We now focus on the stability of Turing patterns, for which we separate the discussion into two cases depending on the shape of the spatial distributions.

Case (I) Striped patterns correspond to

$$(\rho_1, \rho_2, \rho_3) = (\rho, 0, 0), \text{ where } \rho = \sqrt{\mu/g_1}. \tag{5.6}$$

Substituting (5.6) into the perturbation equations (5.5), we have

$$\tau_0 \frac{d}{dt}\begin{pmatrix}\delta\rho_1\\ \delta\rho_2\\ \delta\rho_3\end{pmatrix} = \begin{pmatrix} -2\mu & 0 & 0 \\ 0 & \mu(1-g_2/g_1) & |h|\sqrt{\mu/g_1} \\ 0 & |h|\sqrt{\mu/g_1} & \mu(1-g_2/g_1) \end{pmatrix}\begin{pmatrix}\delta\rho_1\\ \delta\rho_2\\ \delta\rho_3\end{pmatrix}. \tag{5.7}$$

In view of $g_1 = g_2$ defined in (4.7), we have that the three eigenvalues of system (5.7) are

$$\lambda_1 = -2\mu < 0, \ \lambda_2 = -|h|\sqrt{\mu/g_1} < 0, \ \lambda_3 = |h|\sqrt{\mu/g_1} > 0,$$

and therefore striped patterns are not stable and will eventually vanish in the long term.

Case (II) Hexagonal patterns correspond to

$$(\rho_1, \rho_2, \rho_3) = (\rho, \rho, \rho), \text{ where } \rho = \frac{|h| \pm \sqrt{h^2 + 4(g_1+2g_2)\mu}}{2(g_1+2g_2)}. \tag{5.8}$$

Substituting (5.8) into the perturbation equations (5.5), we have

$$\tau_0 \frac{d}{dt}\begin{pmatrix}\delta\rho_1\\ \delta\rho_2\\ \delta\rho_3\end{pmatrix} = \begin{pmatrix}\alpha & \beta & \beta\\ \beta & \alpha & \beta\\ \beta & \beta & \alpha\end{pmatrix}\begin{pmatrix}\delta\rho_1\\ \delta\rho_2\\ \delta\rho_3\end{pmatrix}, \tag{5.9}$$

where $\alpha = \mu - 5g_1\rho^2$, $\beta = |h|\rho - 2g_1\rho^2$. The characteristic equation of (5.9) is

$$(\lambda-\alpha)^3 - 3\beta^2(\lambda-\alpha) - 2\beta^3 = 0,$$

and so the three eigenvalues of system (5.7) are

$$\lambda_1 = \lambda_2 = \mu - |h|\rho - 3g_1\rho^2,\ \ \lambda_3 = \mu + 2|h|\rho - 9g_1\rho^2. \tag{5.10}$$

Substituting $\rho = \frac{|h|\pm\sqrt{h^2+4(g_1+2g_2)\mu}}{2(g_1+2g_2)}$ and $g_1 = g_2$ into (5.10), we have

$$\lambda_1 = \lambda_2 = -\frac{h^2}{3g_1} < 0,\ \ \lambda_3 = -\frac{12g_1\mu + h^2 \pm |h|\sqrt{h^2+12g_1\mu}}{6g_1} < 0.$$

Therefore, hexagonal patterns are stable whenever $\mu > -\frac{h^2}{12g_1}$.

6 Finite volume method and multiresolution-based adaptivity

6.1 Perliminaries and admissible meshes

Let us consider a discretization of the time interval $(0,T)$ by setting $t^n := n\Delta t$ for $n \in \{0,\dots,N\}$, where N is the smallest integer such that $N\Delta t \geq T$. By an *admissible mesh* for Ω we will refer to a family $\mathcal{T}$ of control volumes of maximum diameter h and a family of points $(x_K)_{K\in\mathcal{T}}$ satisfying the following properties (cf. Eymard et al., 2000, Def. 5.1). For a given finite volume $K \in \mathcal{T}$, x_K is its center and $N(K)$ the set of its neighbors (control volumes sharing a common edge with K). We denote by $\mathcal{E}(K)$ the set of edges of K, $\mathcal{E}_{\rm int}(K)$ is the restriction to those in the interior of Ω and $\mathcal{E}_{\rm ext}(K) = \mathcal{E}(K) \setminus \mathcal{E}_{\rm int}(K)$ is the set of edges of K lying on $\partial\Omega$. For every $L \in N(K)$, by $\sigma = K|L$ ($\sigma = K|\partial\Omega$, respectively) we denote the interface between K and L (between K and $\partial\Omega$, respectively). By $\boldsymbol{n}_{K,\sigma}$ we denote the unit normal vector to $\sigma = K|L$ ($\sigma \in \mathcal{E}_{\rm ext}(K)$, respectively) pointing from K to L (from K to $\partial\Omega$, respectively). Moreover, $|K|$ stands for the two-dimensional measure of K and $|\sigma|$ for the one-dimensional measure of $\sigma \in \mathcal{E}$. It is also assumed that

$$\text{the segment } \overline{x_K x_L} \text{ is orthogonal to } \sigma_{K,L} \text{ for every } K, L \in \mathcal{T}. \tag{6.1}$$

6.2 Multiresolution setting

We now introduce a hierarchy of nested admissible meshes $\mathcal{T}^0 \subset \cdots \subset \mathcal{T}^H$ forming a graded tree Λ, in which each grid $\mathcal{T}^l$ is a compound of control volumes K^l of the level l, $l = 0,\dots,H$, where $l = 0$ corresponds to the coarsest and $l = H$ to the finest level of the tree Λ. In order to define a multiresolution framework (Berres and Ruiz-Baier, 2011), for a given control volume K^l we define a *refinement set* by

$$\mathcal{R}_{K^l} := \left\{L_i^{l+1}\right\}_i,$$

where L_i^{l+1} denotes a control volume at the resolution level $l+1$, $L_i^{l+1} \subset K^l$. By definition of the nested hierarchy, it holds that

$$\overline{K^l} := \bigcup_{i=1}^{\#\mathcal{R}_{K^l}} L_i^{l+1}.$$

For $\boldsymbol{x} \in K^l$ the *scale box function* is defined as $\varphi_{K^l}(\boldsymbol{x}) := |K^l|^{-1}\chi_{K^l}(\boldsymbol{x})$ (where χ is the characteristic function), and therefore the average of any function $w(t) \in L^1(\Omega)$ over K^l can be recast as $w_{K^l}(t) = \langle w(t), \varphi_{K^l}\rangle_{L^1(\Omega)}$.

To move between resolution levels, certain transfer operators are needed. With the help of these maps, one can determine an invertible transformation between finite volumes on level $l = H$, and the set formed by finite volumes on the level $l = 0$ and a sequence of *wavelet coefficients*. To switch from fine to coarser levels, a projection operator for cell averages and box functions is defined by

$$w(t)_{K^l} = \sum_{L_i^{l+1}\in\mathcal{R}_{K^l}} \frac{|L_i^{l+1}|}{|K^l|} w(t)_{L_i^{l+1}}, \quad \varphi_{K^l} = \sum_{L_i^{l+1}\in\mathcal{R}_{K^l}} \frac{|L_i^{l+1}|}{|K^l|} \varphi_{L_i^{l+1}},$$

whereas to move from coarse to fine levels we define a polynomial interpolation

$$\tilde{w}(t)_{K^{l+1}} = \sum_{T^l\in\mathcal{S}_K^l} g_{K,T}^l w(t)_{T^l}.$$

The set $\mathcal{S}_K^l$ is a stencil of interpolation (of order s), and $g_{K,T}^l$ are prediction coefficients. Further details on the precise definition of these coefficients and stencils are given in e.g. Bendahmane et al. (2009). For $\boldsymbol{x} \in K^{l+1}$, and depending on the choice of the predictor map, the *wavelet* function is defined as

$$\psi_{K^l,j} = \varphi_{L_i^{l+1}} - \sum_{m=-s}^{s} \tilde{\gamma}_{i+m}\varphi_{L_{i+m}^l} \qquad \text{for } j = 1,\dots,\#\mathcal{R}_{K^l},$$

where $L_i^{l+1} \in \mathcal{R}_{K^l}$, and the value of each $\tilde{\gamma}_{i+m}$ depends on the coefficients $g_{K,T}^l$ of the prediction operator. The difference between the cell average and the predicted value for the scalar $w(t)$ is called wavelet coefficient and is defined by

$$d_{K^l}^w := \left|w(t)_{K^l} - \tilde{w}(t)_{K^l}\right| = \left|\langle w(t), \psi_{K^l}\rangle\right|.$$

Data compression is achieved by discarding all information of control volumes where the local wavelet coefficient is lower than a level-dependent tolerance, i.e.,

$$d_{K^l}^w < \varepsilon_l, \quad l = 0,\dots,H. \tag{6.2}$$

These level-dependent tolerances can be defined so that the error due to thresholding is of the same order as the discretization error induced by the baseline finite volume formulation, therefore preserving the order of the base scheme (Berres and Ruiz-Baier, 2011).

Remark 1 The key concept of the fully adaptive strategy of multiresolution consists in defining an evolving set of leaves $\mathcal{L}(\Lambda)$ of the tree Λ, formed by all tree nodes K^l that are not discarded by the thresholding defined in (6.2), and such that all cells in $\mathcal{R}_{K^l}$ satisfy (6.2). Then, the underlying discrete scheme is first defined on $\mathcal{L}(\Lambda)$. However, $\mathcal{L}(\Lambda)$ *is not an admissible mesh* in general, and therefore an auxiliary set of nodes, called *virtual leaves* is required in order to fullfil (6.1).

The set of virtual leaves consists in cells of $\Lambda \setminus \mathcal{L}(\Lambda)$ that for a given $K^l \in \mathcal{L}(\Lambda)$, belong to $N(K^l) \cap \mathcal{T}^l$. We will denote by $\tilde{\mathcal{L}}(\Lambda)$ the set formed by leaves and virtual leaves. In addition, the set Λ_d of cells marked as *deletable* consists in all elements that satisfy (6.2). Virtual leaves are needed to evaluate numerical fluxes on each leaf.

6.3 Multiresolution - Finite volume formulation

The baseline finite volume discretization of (1.2) is based on the so-called shifted Grünwald approximation of local gradients (see e.g. Meerschaert and Tadjeran, 2006; Yang et al., 2010). Irrespective of the specific form of the gradient approximation, the property of local flux conservation yields the following expression for a first order finite volume approximation of the fractional diffusion operator applied to a generic scalar field w over the finest-level cell K^H at time t^n:

$$-\widetilde{\Delta^{\gamma/2}} := -\Delta^{\gamma/2} w^n_{K^H} \approx -\sum_{L_i \in \mathcal{H}(K^H)} g_{\gamma,L_i} \frac{|\sigma_{K^H,L_i}|}{d_{K^H,L_i}} \big(w^n_{L_i} - w^n_{K^H}\big), \tag{6.3}$$

where $g_{\gamma,L_i}, \mathcal{H}$ are, respectively, particular weights and approximation stencil which we will precisely defined in terms of Cartesian grids, for sake of clarity. Let us assume a square domain Ω discretized into $N_x \times N_y$ equally sized boxes of area $h_x h_y$, and notice that (6.3) can be written as

$$-\widetilde{\Delta^{\gamma/2}} w^n_{ij} = -\frac{1}{h_x^\gamma} \sum_{k=0}^{i+1} g_{\gamma,k} w^n_{i-k+1,j} - \frac{1}{h_y^\gamma} \sum_{l=0}^{j+1} g_{\gamma,l} w^n_{i,j-l+1},$$

where $g_{\gamma,m} := (-1)^m \binom{\gamma}{m}$, (see also Concezzi and Spigler, 2012). These considerations imply that the fully explicit Euler FV discrete analogue of (1.2) defined on the finest mesh reads: Starting from a L^2-average of the initial data

$$u^0_{K^H} = \frac{1}{|K^H|} \int_{K^H} u_0(x)\, dx, \quad v^0_{K^H} = \frac{1}{|K^H|} \int_{K^H} v_0(x)\, dx, \forall K^H \in \mathcal{T}^H,$$

and for every $n = 0, \ldots$, recursively find $u^{n+1}_{K^H}, v^{n+1}_{K^H}$ such that

$$\begin{aligned} |K^H| \frac{u^{n+1}_{K^H} - u^n_{K^H}}{\Delta t} - d_{11} \widetilde{\Delta^{\gamma/2}} u^n_{K^H} - d_{12} \widetilde{\Delta^{\gamma/2}} v^n_{K^H} &= |K| F^n_{K^H}, \\ |K^H| \frac{v^{n+1}_{K^H} - v^n_{K^H}}{\Delta t} - d_{22} \widetilde{\Delta^{\gamma/2}} v^n_{K^H} &= |K| G^n_{K^H}, \end{aligned} \tag{6.4}$$

where $F^n_{K^H}, G^n_{K^H}$ are explicit approximations of the reaction terms over each control volume

$$\frac{1}{|K^H|} \int_K F\big(u(x,t^n), v(x,t^n)\big)\, dx, \quad \frac{1}{|K^H|} \int_K G\big(u(x,t^n), v(x,t^n)\big)\, dx,$$

and are given by

$$F^n_{K^H} = F\big({u^n_{K^H}}^+, {v^n_{K^H}}^+\big), \quad G^n_{K^H} = G\big({u^n_{K^H}}^+, {v^n_{K^H}}^+\big).$$

We stress that if K^l is a leaf, then the unknowns are computed from the MRFV method (6.4), whereas if K^l is a virtual leaf, the values of each species concentration are simply obtained by the MR transform of their values at lower refinement levels. The multiresolution transform and thresholding strategy are summarized in Algorithm 1.

7 A numerical example

For numerically studying the pattern formation of system (1.1), it suffices to consider the dynamics induced by small-amplitude perturbations to the homogeneous steady state. The domain is confined to the square $\Omega = [0, 50] \times [0, 50]$, and it is discretized using a Cartesian mesh consisting of 262,144 cells in the highest resolution level $H = 9$, and the time step is

Algorithm 1 – Multiresolution transform and thresholding.

set level-dependent threshold ε_l
set values $u^n_{K^H}, v^n_{K^H}$ on the finest level of Λ
for $l = H-1,\dots,1$ **do**
  for $K^l \in \mathcal{T}^l$ **do**
    Compute $u^n_{K^l} = \sum_{L_i^{l+1}\in\mathcal{R}_{K^l}} \frac{|L_i^{l+1}|}{|K^l|} u^n_{K^{l+1}}$, $v^n_{K^l} = \sum_{L_i^{l+1}\in\mathcal{R}_{K^l}} \frac{|L_i^{l+1}|}{|K^l|} v^n_{K^{l+1}}$.
  end for
end for
for $l = 1,\dots,H-1$ **do**
  for $K^l \in \mathcal{T}^l$ **do**
    Compute

$$u^{n,*}_{K^l} = \sum_{T^{l-1}\in\mathcal{S}_K^{l-1}} g^{l-1}_{K,T} u^n_{K^{l-1}},\ v^{n,*}_{K^l} = \sum_{T^{l-1}\in\mathcal{S}_K^{l-1}} g^{l-1}_{K,T} v^n_{K^{l-1}},\ \boldsymbol{d}^n_{K^l} = \|u^n_{K^l} - u^{n,*}_{K^l}\| + \|v^n_{K^l} - v^{n,*}_{K^l}\|,$$

    if $\boldsymbol{d}^n_{K^l} < \varepsilon_l$ **then**
      Add $L_i^{l+1} \in \mathcal{R}_{K^l}$ to the set of deletable cells Λ_d
    end if
  end for
end for
for $l = H-1,\dots,1$ **do**
  for $K^l \in \mathcal{T}^l$ **do**
    if $K^l \in \Lambda_d$ **and** $L^{l+1} \in \mathcal{R}_{K^l} \cap \Lambda_d \cap \mathcal{L}(\Lambda)$ **then**
      Remove L^{l+1} from the tree Λ.
    end if
    if $K^l \notin \Lambda_d$ **and** $l < H$ **then**
      Add L^{l+1} to the tree Λ.
    end if
  end for
end for

$\Delta t = 0.005$. The model parameters are set to $\gamma = 1$, $a = 1.2$, $b = 1$, $c = 0.5$, $d_{11} = d_{22} = 1$, $d_{12} = 5.02$, and the reference tolerance required for the thresholding algorithm is $\varepsilon_{\mathrm{R}} = 0.0001$. The initial data is taken as

$$u(x,0) = u^* + \eta_1(x), \quad v(x,0) = v^* + \eta_2(x), \tag{7.1}$$

where $\eta_1 \in [-0.05, 0.05]$ and $\eta_2 \in [-0.025, 0.025]$ are uniformly distributed random perturbations and (u^*, v^*) is the equilibrium state. The time evolution of the perturbed initial state (7.1) is displayed in Figure 4, where we can observe convergence to hexagonally-shaped spatial patterns. Note that in the case of normal diffusion, the system is expected to exhibit a regime of self-replicating spots, as discussed in e.g. Pearson (1993). We also depict sketches of the meshes generated by the multiresolution strategy (see the bottom row of Figure 4), which after successive local refinement and coarsening clearly identify the zones of high solution gradients. The multiresolution method also allows substantial reduction in computational burden due to the fast MR transform and graded tree structure (Bendahmane et al., 2009). We also present an analogous test where we have only modified the order of the fractional diffusion to $\gamma = 1.5$, and we can observe substantial differences in terms of spatial distribution of patterns. The approximate solutions along with fully adaptive meshes are presented in Figure 5.

8 Concluding remarks

We have introduced the Lévy flights type of superdiffusion into a Lotka-Volterra competitive model. A stability analysis yields as conclusion that cross superdiffusion gives rise to Turing instability while self superdiffusion suppresses Turing instability. Moreover, after applying a

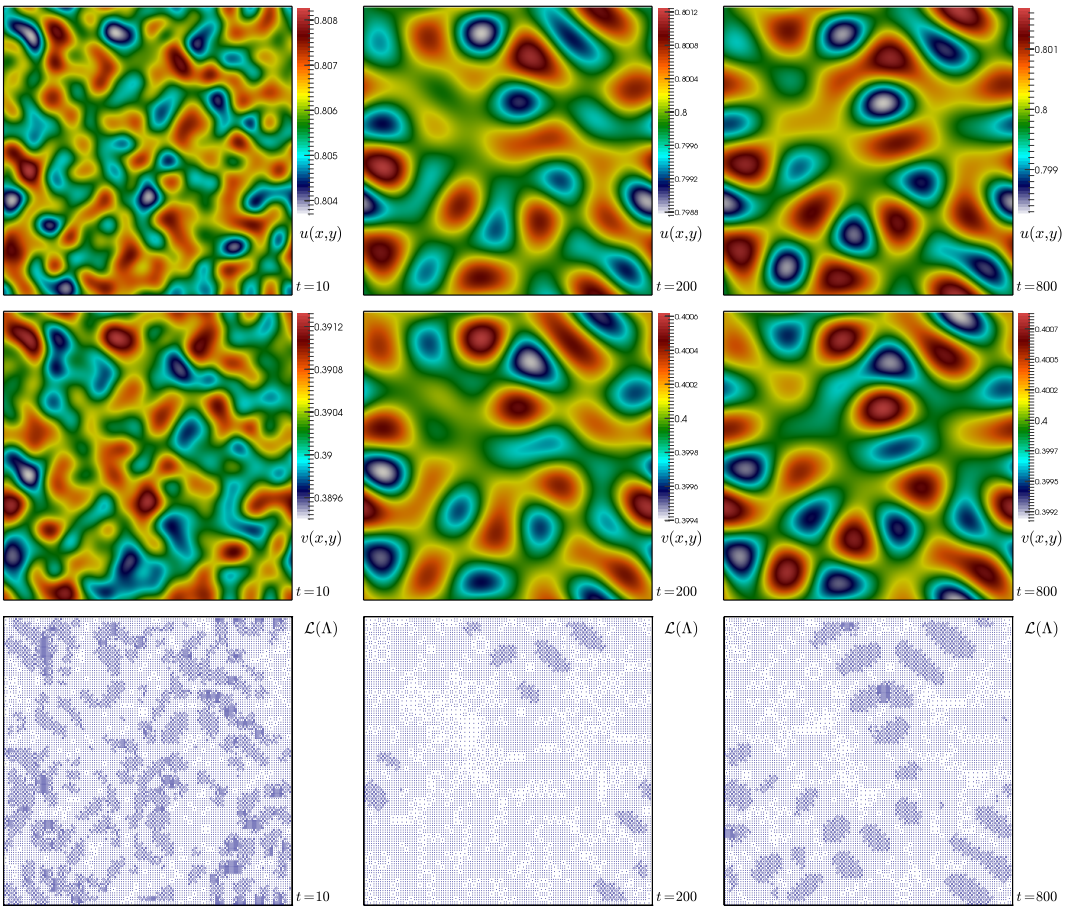

Fig. 4 Snapshots at $t = 10, 200, 800$ (left, center, right, respectively) of the Turing pattern formation for species u, v (top and middle, respectively) in the case where the order of Weyl fractional operator is $\gamma = 1$. The employed parameters are $a = 1.2$, $b = 1$, $c = 0.5$, $d_{11} = d_{22} = 1$, $d_{12} = 5.02$. The bottom panels exhibit snapshots of the mass center of leaves in the adaptively refined meshes generated with the multiresolution algorithm with a global threshold of $\varepsilon_{\mathrm{R}} = 0.0001$.

weakly nonlinear analysis, we can also assert that the Turing patterns are stable hexagons. An immediate application of these observations from the viewpoint of biology, is that when the inter-population competition is larger than the intra-population competition, the reached inhomogeneous steady state is stable.

Acknowledgement

RRB gratefully acknowledges the support by the Swiss National Science Foundation through the research grant PP00P2_144922. CT acknowledges partial support by the PRC grant NSFC 11201406 and by the Qinglan Project.

References

Andreianov B, Bendahmane M, and Ruiz-Baier R (2011) Analysis of a finite volume method for a cross-diffusion model in population dynamics. *Math. Models Methods Appl. Sci.* **21**:307–

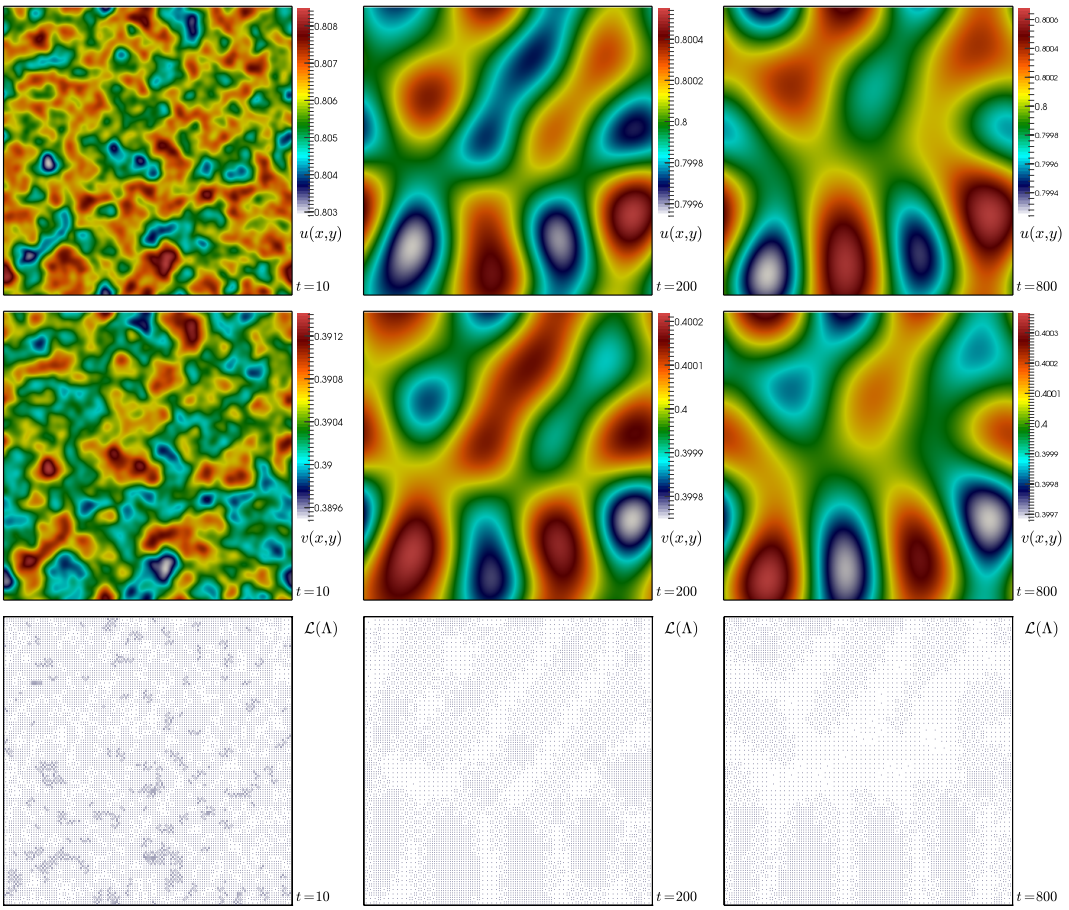

Fig. 5 Snapshots at $t = 10, 200, 800$ (left, center, right, respectively) of the Turing pattern formation for species u, v (top and middle, respectively) in the case where the order of Weyl fractional operator is $\gamma = 1.5$. The remaining parameters are chosen as in the previous example. The bottom panels show snapshots of the mass center of leaves in the adaptively refined meshes generated with the multiresolution algorithm with a global threshold of $\varepsilon_{\mathrm{R}} = 0.0001$.

344

Bendahmane M (2010) Weak and classical solutions to predator-prey system with cross-diffusion. *Nonlinear Anal.* **73**(8):2489–2503

Bendahmane M, Bürger R, Ruiz-Baier R, and Schneider K (2009) Adaptive multiresolution schemes with local time stepping for two-dimensional degenerate reaction-diffusion systems. *Appl. Numer. Math.* **59**:1668–1692

Bendahmane M and Karlsen KH (2006) Analysis of a class of degenerate reaction-diffusion systems and the bidomain model of cardiac tissue. *Netw. Heterog. Media* **1**(1):185–218

Berres S and Ruiz-Baier R (2011) A fully adaptive numerical approximation for a two-dimensional epidemic model with nonlinear cross-diffusion. *Nonl. Anal. Real World Appl.* **12**:2888–2903

Bouchard JP and Georges A (1990) Anomalous diffusion in disordered media: Statistical mechanics, model and physical application. *Phys. Rep.* **195**:127–293

Concezzi M and Spigler R (2012) Numerical solution of two-dimensional fractional diffusion equations by a high-order ADI method. *Commun. Appl. Ind. Math.* **3**(2):e-421

Eymard R, Gallouët T, and Herbin R (2000) Finite Volume Methods. In Ciarlet, P.G., and Lions, J.L. (eds.), Handbook of Numerical Analysis, vol. VII, North-Holland, Amsterdam, pp. 713–1020

Gafiychuk VV and Datsko BY (2006) Pattern formation in a fractional reaction-diffusion system. *Phys. A* **365**:300–306

Gambino G, Lombardo MC, Sammartino M, and Sciacca V (2013) Turing pattern formation in the Brusselator system with nonlinear diffusion. *Phys. Rev. E* **88**:042925

Golovin AA, Matkowsky BJ, and Volpert VA (2008) Turing pattern formation in the Brusselator model with superdiffusion. *SIAM J. Appl. Math.* **69**:251–272

Henry BI, Langlands TAM, and Wearne SL (2005) Turing pattern formation in fractional activator-inhibitor systems. *Phys. Rev. E* **72**:026101

Henry BI and Wearne SL (2002) Existence of Turing instabilities in a two-species fractional reaction-diffusion system. *SIAM J. Appl. Math.* **62**:870–887

Horstmann D (2007) Remarks on some Lotka–Volterra type cross-diffusion models. *Nonlinear Anal. Real World Appl.* **8**:90–117

Jüngel A (2010) *Diffusive and nondiffusive population models, Mathematical Modeling of Collective Behavior in Socio-Economic and Life Sciences*, Boston: Birkhäuser

Langlands TAM, Henry BI, and Wearne SL (2007) Turing pattern formation with fractional diffusion and fractional reactions. *J. Physics: Condensed Matter* **19**:065115

Li BW and Wang J (2003) Anomalous heat conduction and anomalous diffusion in one-dimensional systems. *Phys. Rev. Lett.* **91**:044301

Lou Y and Ni WM (1996) Diffusion, self-diffusion and cross-diffusion. *J. Diff. Eqs.* **131**:79–131

Lou Y, Nagylaki T, and Ni WM (2001) On diffusion-induced blowups in a mutualistic model. *Nonlin. Anal.: Theory Meth. Appl.* **45**:329–342

Meerschaert MM, and Tadjeran C (2006) Finite difference approximations for two-sided space-fractional partial differential equations. *Appl. Numer. Math.* **5**(6):80–90

Metzler R and Klafter J (2000) The random walk's guide to anomalous diffusion: a fractional dynamics approach. *Phys. Rep* **339**:1–77

Metzler R and Klafter J (2004) The restaurant at the end of the random walk: recent developments in the description of anomalous transport by fractional dynamics. *J. Phys. A* **37**:R161

Nec Y, Nepomnyashchy AA, and Golovin AA (2008) Oscillatory instability in super-diffusive reaction-diffusion systems: Fractional amplitude and phase diffusion equations. *Europhys. Letters* **82**:58003

Okubo A and Levin S (2002) *Diffusion and Ecological Problems: Modern Perspectives*. Springer, New York

Pearson JE (1993) Complex patterns in a simple system. *Science* **261**:189–192

Kruzhkov SN (1969) Results on the nature of the continuity of solutions of parabolic equations and some of their applications. *Mat. Zametki* **6**(1):97–108; English tr. in *Math. Notes* **6**(1):517–523

Schmitt FG and Seuront L (2001) Multifractal random walk in copepod behavior. *Phys. A* **301**:375–396

Sokolov IM, Klafter J, and Blumen A (2002) Fractional kinetics. *Physics Today* **55**:48–54

Toner J, Tu Y, and Ramaswamy S (2005) Hydrodynamics and phases of flocks. *Annals of Physics* **318**:170–244

Viswanathan GM and Afanasyevt V (1996) Lévy flight search patterns of wandering albatrosses. *Nature* **381**:30

Weiss M, Hashimoto H, and Nilsson T (2003) Anomalous protein diffusion in living cells as seen by fluorescence correlation spectroscopy. *Biophys J.* **84**:4043–4052

Yang Q, Liu F, and Turner I (2010) Numerical methods for fractional partial differential equations with Riesz space fractional derivatives. *Appl. Numer. Model.* **34**:200–218